where α_i and β_j are parameters. The residual vectors, $|\delta_i\rangle$ and $|\delta_j\rangle$, are expected to lack the evolutionary information of the source organisms. Note that $|\nu_j\rangle$ is excluded from the summation on the right side of the equation (8). Likewise, $|\nu_i\rangle$ is excluded from the summation on the right side of the equation (9). The similarity between the two residual vectors is considered to indicate the intensity of co-evolution between proteins i and j. To evaluate the similarity between the residual vectors, the Pearson's correlation coefficient between $|\delta_i\rangle$ and $|\delta_j\rangle$ was calculated. As described above, the inner product between the normalized residual vectors is equivalent to the Pearson's correlation coefficient between them:

$$\rho_{ij}^{\mathrm{PARTIAL}} = \langle \delta_i^{\#} | \delta_j^{\#} \rangle. \tag{10}$$

The correlation coefficient is called the partial correlation coefficient between $|\nu_i\rangle$ and $|\nu_j\rangle$. In actual practice, the following formula was used to obtain the partial correlation coefficient, instead of performing multiple regression.

$$\rho_{ij}^{\mathrm{PARTIAL}} = \frac{-(R^{-1})_{ij}}{\sqrt{(R^{-1})_{ii}}\sqrt{(R^{-1})_{jj}}}, \tag{11}$$

where R is the correlation coefficient matrix whose (i,j)-th element is $\rho_{ij}^{\mathrm{MIRROR}}$, and the superscript -1 indicates inverse. ρ^{PARTIAL} without subscripts, i and j, collectively represents that the type is partial correlation coefficient.

3 Results and Discussions

We calculated five types of correlation coefficients, ρ^{MIRROR}, ρ^{16S}, ρ^{AVE}, ρ^{PC1} and ρ^{PARTIAL}, for all of the possible pairs of 26 proteins, that is, 325 pairs of proteins. The performance of each correlation coefficient was evaluated with specificity and sensitivity. Out of the 325 pairs, the interactions of 13 pairs have been experimentally identified. Only top 20 of the five types of correlation coefficients are shown in Table 1, where the actually interacting pairs are highlighted with circles. As shown in the table, the top ranks of ρ^{16S}, ρ^{AVE}, ρ^{PC1} and ρ^{PARTIAL} were occupied by pairs of actually interacting proteins. In contrast, non-interacting proteins were present within the top ranks of ρ^{MIRROR}. The decreasing patterns of the five correlation coefficients are seen in this table. The decrease of ρ^{MIRROR} was quite slow, whereas ρ^{AVE}, ρ^{PC1} and ρ^{PARTIAL} decreased rapidly. The rate of the ρ^{16S} decrease was rather moderate. The decreasing patterns shown in Table 1 clearly demonstrates the problem of the original mirror tree method. Even if a high value, e.g. 0.9, is used as a threshold for the correlation coefficient to predict a protein–protein interaction, ρ^{MIRROR} produces many pairs with high correlation, including non-interacting pairs, which likely lead to the generation of many false positives. However, the occupation of the top ranks by interacting proteins and the rapid decreases of ρ^{16S}, ρ^{AVE}, ρ^{PC1} and ρ^{PARTIAL} guarantee the specificity of prediction, if the threshold is set at a sufficiently high value.

Table 1. Comparison of top 20 protein pairs sorted in decreasing order of the correlation coefficients

rank	ρ^{MIRROR}		ρ^{16S}		ρ^{AVE}		ρ^{PC1}		ρ^{PARTIAL}	
1	dnaN-rpoB	0.977	sucD-sucC	0.924 O	sucD-sucC	0.910 O	sucD-sucC	0.915 O	sucD-sucC	0.885 O
2	dnaK-secY	0.963	atpA-atpD	0.803 O	trpA-trpB	0.792 O	trpA-trpB	0.754 O	trpA-trpB	0.744 O
3	dnaK-rpoB	0.963	carA-carB	0.803 O	rpoA-rpoB	0.654 O	carA-carB	0.649 O	tufB-tsf	0.612 O
4	sucD-sucC	0.962 O	dnaK-secY	0.801	carA-carB	0.642 O	atpA-atpD	0.640 O	carA-carB	0.597 O
5	dnaN-dnaK	0.960	trpA-trpB	0.797 O	dnaN-rpoB	0.634	dnaN-rpoB	0.587	rpoA-carA	0.519
6	atpA-atpD	0.959 O	dnaE-secA	0.783	atpA-atpD	0.615 O	dnaK-atpD	0.560	dnaN-iscS	0.505
7	rpoA-rpoB	0.958 O	dnaK-atpD	0.774	iscS-iscU	0.607 O	dnaK-secY	0.560	grpE-rpoB	0.462
8	rpoB-secY	0.955	dnaN-rpoB	0.772	grpE-clpP	0.553	iscS-iscU	0.555 O	dnaK-secY	0.457
9	secY-secA	0.954 O	rpoA-rpoB	0.768 O	dnaK-carB	0.541	grpE-clpP	0.545	rpoA-rpoB	0.450 O
10	dnaK-atpD	0.953	dnaN-carA	0.761	grpE-tsf	0.541	dnaK-carB	0.542	atpA-atpD	0.443 O
11	dnaN-secY	0.953	dnaN-dnaK	0.760	dnaK-secY	0.516	secY-carB	0.531	ruvA-ruvB	0.439 O
12	dnaK-atpA	0.952	dnaK-carB	0.758	dnaK-atpD	0.514	dnaK-rpoB	0.500	dnaA-dnaB	0.358 O
13	dnaE-secA	0.945	dnaN-secY	0.758	ruvA-ruvB	0.511 O	rpoA-rpoB	0.498 O	grpE-dnaN	0.355
14	dnaN-rpoA	0.945	dnaE-secY	0.755	secY-carB	0.501	grpE-tsf	0.497	clpP-atpD	0.345
15	dnaK-secA	0.944	rpoB-secY	0.753	rpoB-secY	0.498	dnaK-atpA	0.496	dnaK-tufB	0.339
16	dnaE-secY	0.944	dnaK-atpA	0.747	tsf-trpB	0.476	ruvA-ruvB	0.489 O	dnaB-sucD	0.336
17	dnaN-clpX	0.943	dnaE-dnaK	0.743	dnaA-ruvB	0.469	dnaE-secA	0.480	secA-carB	0.333
18	dnaN-secA	0.940	secY-carB	0.727	secA-trpB	0.453	dnaE-secY	0.477	dnaK-sucC	0.329
19	clpX-rpoB	0.937	iscS-iscU	0.717 O	tufB-tsf	0.445 O	dnaA-ruvB	0.455	atpA-sucC	0.306
20	dnaN-carA	0.937	dnaK-carA	0.716	dnaK-atpA	0.438	secY-secA	0.431 O	clpX-dnaE	0.302

The abbreviated names of the interacting proteins are as follows: sucC-sucD, succinyl-CoA synthetases alpha - beta: atpA-atpD. ATP synthases alpha - beta; rpoA-rpoB, DNA - directed RNA polymerases alpha - beta; secA-secY, preprotein translocase secA - secY: carA-carB, carbamoyl-phosphate synthases small - large; ruvA-ruvB, Holliday junction DNA helicases ruvA - ruvB; iscS-iscU, putative aminotransferase - NifU-like protein; dnaE-dnaN, DNA polymerases III alpha - beta; trpA-trpB, tryptophan synthases alpha - beta: tufB-tsf, elongation factors EF-Tu - EF-Ts; dnaA-dnaB, DNA helicase - dnaA; grpE-dnaK, heat shock protein grpE - dnaK protein: and clpX-clpP, ATP-dependent clp proteases ATP-binding subunit - protease proteolytic subunit.

The unit vector $|u\rangle$ seems to be a crucial factor for the prediction of a protein protein interaction when a projection operator is used. Therefore, we examined the relationships among $|u_{16S}\rangle$, $|u_{AVE}\rangle$ and $|u_{PC1}\rangle$ by calculating absolute value of Pearson's correlation coefficients $|r|$ among them. $|r|$ between $|u_{16S}\rangle$ and $|u_{AVE}\rangle$ was 0.947, whereas $|r|$ between $|u_{16S}\rangle$ and $|u_{PC1}\rangle$ was 0.946. The highest correlation, $|r| = 0.998$, was observed between $|u_{AVE}\rangle$ and $|u_{PC1}\rangle$. The high correlation between $|u_{16S}\rangle$ and the other unit vectors suggests that the information except for the evolutionary relationship of source organisms can be approximately canceled out by the average operation or principal component analysis.

The ρ^{16S}, ρ^{AVE}, ρ^{PC1} and $\rho^{PARTIAL}$ seem to outperform the ρ^{MIRROR}. That is, the exclusion of the information about the evolutionary relationships among the source organisms from the distance matrices is effective to reduce the number of the false positives from the mirror tree predictions. The specificities and the sensitivities of the five types of correlation coefficients under four different threshold values, 0.9, 0.8, 0.7 and 0.6, are shown in Table 2. When a pair of proteins had a correlation coefficient greater than the threshold the proteins were predicted to interact with each other. Three types of correlation coefficients, ρ^{AVE}, ρ^{PC1} and $\rho^{PARTIAL}$, showed high specificity under any threshold value, whereas ρ^{16S} showed high specificity only when threshold was 0.9 or 0.8. The high specificities of ρ^{16S}, ρ^{AVE}, ρ^{PC1} and $\rho^{PARTIAL}$ mean the drastic reduction of false positives, compared with ρ^{MIRROR} [18,19]. Recently, Pazos *et al.* [13] have independently developed a method to exclude the information of evolutionary relationship among the source organisms by using 16S rRNA. They adjust the scale of the distance matrix of rRNA to that of the distance matrix of a protein, and simply subtract the former from the latter. Then, correlation coefficient is calculated between the sets of residual elements. Improvement in specificity is also observed by their operation, although the mathematical framework of their method is different from those of ours.

Table 2. Specificity and Sensitivity of the prediction

Method	Specificity				Sensitivity			
	0.9	0.8	0.7	0.6	0.9	0.8	0.7	0.6
ρ^{MIRROR}	13.79	6.21	4.96	4.17	61.54	84.62	100.00	100.00
ρ^{16S}	100.00	75.00	28.57	24.32	7.14	21.43	42.86	64.29
ρ^{AVE}	100.00	100.00	100.00	85.71	7.14	7.14	14.29	42.86
ρ^{PC1}	100.00	100.00	100.00	100.00	7.14	7.14	14.29	28.57
$\rho^{PARTIAL}$	-	100.00	100.00	100.00	0.00	7.14	14.29	21.43

$$\text{Specificity} = \frac{\text{true positive}}{(\text{true positive} + \text{false positive})} \times 100\%,$$

$$\text{Sensitivity} = \frac{\text{true positive}}{(\text{true positive} + \text{false negative})} \times 100\%.$$

When threshold was set to 0.9, no interacting pair was predicted with $\rho^{PARTIAL}$, and specificity was not calculated in the case.

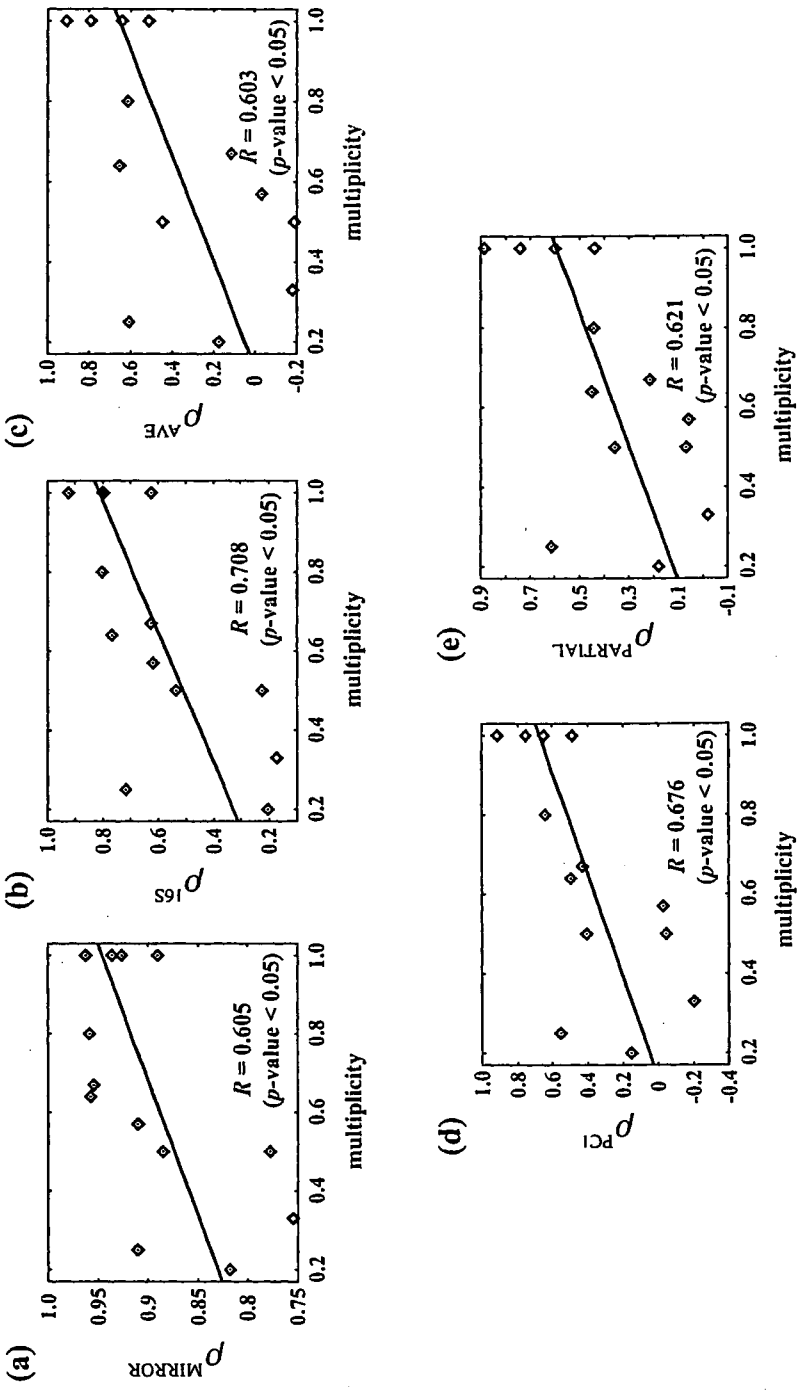

Fig. 1. The relationship between multiplicity and five types of correlation coefficients, ρ^{MIRROR}, ρ^{16S}, ρ^{AVE}, ρ^{PC1} and ρ^{PARTIAL}

Despite the improvement described above, the sensitivities of ρ^{16S}, ρ^{AVE}, ρ^{PCT} and $\rho^{PARTIAL}$ were lower than that of ρ^{MIRROR}. This means that a pair of proteins i and j did not always show high ρ_{ij}^{16S}, ρ_{ij}^{AVE}, ρ_{ij}^{PCT} and $\rho_{ij}^{PARTIAL}$ even when proteins, i and j, interact with each other. In other words, the number of false negatives increased when our methods were used, compared with the original mirror tree method. Here, we calculated the intensity of co-evolution between a pair of proteins as the correlation coefficient after excluding the information about the evolutionary relationship among the source organisms from the phylogenetic vectors. However, the pairs may also interact with other proteins. If such proteins exist, it would be difficult to detect the interaction with the pair, because the co-evolution with the other partners may function as noise for the prediction of interaction of a pair. To examine this hypothesis, we investigated the relationship between the multiplicity of the interaction [19] and the correlation coefficient (Fig 1). The multiplicity, or a modified Jaccard coefficient, is a measure defined between a pair of interacting proteins. Consider an interacting pair of proteins A and B. Let M and N be the sets of interaction partners of proteins A and B. The information about the interaction partners were obtained from the DIP database [17]. Protein B belongs to M, whereas N includes protein A. The multiplicity between proteins, A and B, is defined as follows:

$$\text{Multiplicity (modified Jaccard coefficient)} = \frac{|\mathbf{M} \cap \mathbf{N}| + 1}{|\mathbf{M} \cup \mathbf{N}| - 1}. \qquad (12)$$

When proteins A and B interact each other without other interaction partners, multiplicity takes a value 1. When proteins A and B have other interaction partners, the multiplicity decreases. However, when proteins A and B share the other interaction partners, the multiplicity takes a value close to 1. In contrast, when proteins A and B have their own interaction partners respectively, the multiplicity is close to 0. As shown in Fig. 1, the intensities of co-evolution calculated by any method show positive correlation with the multiplicity. That is, the intensities of co-evolution were high when proteins A and B formed a complex without other interaction partners or share the other interaction partners. When proteins A and B had their own interaction partners, that is, the multiplicity was low, the intensities of co-evolution were low. The observation suggests that the false negatives are generated by the presence of unshared interaction partners. Further accumulation of experimental knowledge is required to ascertain this hypothesis.

4 Conclusion

The mirror tree method is a simple approach for the prediction of protein–protein interactions. Here, we reviewed our methods to improve the performance of the original mirror tree method. In the experiment, we confirmed that our methods could drastically reduce the number of false positives in the prediction. Our method, however, generated more false negatives than the original mirror tree method. Our analysis suggested that the presence of unshared interaction

partners may be the cause of the false negatives. However, if we select protein pairs with a high correlation coefficient, e.g. > 0.8, by any one of our methods, we can predict interacting protein pairs with high reliability.

Acknowledgments. This work was supported by Grants-in-Aid for Scientific Research on Priority Areas 'Systems Genomics' (K.H.), 'Comprehensive Genomics' (M.K.) and 'Membrane Interface' (H.T.) from the Ministry of Education, Culture, Sports, Science and Technology of Japan. The computational resource was provided by the Bioinformatics Center, Institute for Chemical Research, Kyoto University.

References

1. Cole, J.R., Chai, B., Farris, R.J., Wang, Q., Kulam-Syed-Mohideen, A.S., McGarrell, D.M., Bandela, A.M., Cardenas, E., Garrity, G.M., Tiedje, J.M.: The ribosomal database project (RDP-II): introducing myRDP space and quality controlled public data. Nucleic Acids Res. 35, D169–D172 (2007)
2. Felsenstein, J.: PHYLIP (Phylogeny Inference Package) version 3.6. Distributed by the author. Department of Genome Sciences, University of Washington, Seattle (2004)
3. Gavin, A.C., Bosche, M., Krause, R., Grandi, P., Marzioch, M., Bauer, A., Schultz, J., Rick, J.M., Michon, A.M., Cruciat, C.M., Remor, M., Hofert, C., Schelder, M., Brajenovic, M., Ruffner, H., Merino, A., Klein, K., Hudak, M., Dickson, D., Rudi, T., Gnau, V., Bauch, A., Bastuck, S., Huhse, B., Leutwein, C., Heurtier, M.A., Copley, R.R., Edelmann, A., Querfurth, E., Rybin, V., Drewes, G., Raida, M., Bouwmeester, T., Bork, P., Seraphin, B., Kuster, B., Neubauer, G., Superti-Furga, G.: Functional organization of the yeast proteome by systematic analysis of protein complexes. Nature 415, 141–147 (2002)
4. Gertz, J., Elfond, G., Shustrova, A., Weisinger, M., Pellegrini, M., Cokus, S., Rothschild, B.: Inferring protein interactions from phylogenetic distance matrices. Bioinformatics 19, 2039–2045 (2003)
5. Goh, C.S., Bogan, A.A., Joachimiak, M., Walther, D., Cohen, F.E.: Co-evolution of proteins with their interaction partners. J. Mol. Biol. 299, 283–293 (2000)
6. Ho, Y., Gruhler, A., Heilbut, A., Bader, G.D., Moore, L., Adams, S.L., Millar, A., Taylor, P., Bennett, K., Boutilier, K., Yang, L., Wolting, C., Donaldson, I., Schandorff, S., Shewnarane, J., Vo, M., Taggart, J., Goudreault, M., Muskat, B., Alfarano, C., Dewar, D., Lin, Z., Michalickova, K., Willems, A.R., Sassi, H., Nielsen, P.A., Rasmussen, K.J., Andersen, J.R., Johansen, L.E., Hansen, L.H., Jespersen, H., Podtelejnikov, A., Nielsen, E., Crawford, J., Poulsen, V., Sorensen, B.D., Matthiesen, J., Hendrickson, R.C., Gleeson, F., Pawson, T., Moran, M.F., Durocher, D., Mann, M., Hogue, C.W., Figeys, D., Tyers, M.: Systematic identification of protein complexes in *Saccharomyces cerevisiae* by mass spectrometry. Nature 415, 180–183 (2002)
7. Ito, T., Chiba, T., Ozawa, R., Yoshida, M., Hattori, M., Sakaki, Y.: A comprehensive two-hybrid analysis to explore the yeast protein interactome. In: Proc. Natl. Acad. Sci. USA 98, pp. 4569–4574 (2001)
8. Jones, D.T., Taylor, W.R., Thornton, J.M.: The rapid generation of mutation data matrices from protein sequences. Comput. Appl. Biosci. 8, 275–282 (1992)

9. Jothi, R., Cherukuri, P.F., Tasneem, A., Przytycka, T.M.: Co-evolutionary analysis of domains in interacting proteins reveals insights into domain-domain interactions mediating protein-protein interactions. J. Mol. Biol. 362, 861–875 (2006)
10. Kanehisa, M., Goto, S., Hattori, M., Aoki-Kinoshita, K.F., Itoh, M., Kawashima, S., Katayama, T., Araki, M., Hirakawa, M.: From genomics to chemical genomics: new developments in KEGG. Nucleic Acids Res. 34, D354–D357 (2006)
11. Katoh, K., Kuma, K., Toh, H., Miyata, T.: MAFFT version 5: improvement in accuracy of multiple sequence alignment. Nucleic Acids Res. 33, 511–518 (2005)
12. Kishino, H., Hasegawa, M.: Evaluation of the maximum likelihood estimate of the evolutionary tree topologies from DNA sequence data, and the branching order in hominoidea. J. Mol. Evol. 29, 170–179 (1989)
13. Pazos, F., Ranea, J.A., Juan, D., Sternberg, M.J.: Assessing protein co-evolution in the context of the tree of life assists in the prediction of the interactome. J. Mol. Biol. 352, 1002–1015 (2005)
14. Pazos, F., Valencia, A.: In silico two-hybrid system for the selection of physically interacting protein pairs. Proteins 47, 219–227 (2002)
15. Pazos, F., Valencia, A.: Similarity of phylogenetic trees as indicator of protein–protein interaction. Protein Eng. 14, 609–614 (2001)
16. Ramani, A., Marcotte, E.M.: Exploiting the co-evolution of interacting proteins to discover interaction specificity. J. Mol. Biol. 327, 273–284 (2003)
17. Salwinski, L., Miller, C.S., Smith, A.J., Pettit, F.K., Bowie, J.U., Eisenberg, D.: The Database of Interacting Proteins: 2004 update. Nucleic Acids Res. 32, D449–D451 (2004)
18. Sato, T., Yamanishi, Y., Horimoto, K., Kanehisa, M., Toh, H.: Partial correlation coefficient between distance matrices as a new indicator of protein-protein interactions. Bioinformatics 22, 2488–2492 (2006)
19. Sato, T., Yamanishi, Y., Kanehisa, M., Toh, H.: The inference of protein-protein interactions by co-evolutionary analysis is improved by excluding the information about the phylogenetic relationships. Bioinformatics 21, 3482–3489 (2005)
20. Sprinzak, E., Sattath, S., Margalit, H.: How reliable are experimental protein–protein interaction data? J. Mol. Biol. 327, 919–923 (2003)
21. Uetz, P., Giot, L., Cagney, G., Mansfield, T.A., Judson, R.S., Knight, J.R., Lockshon, D., Narayan, V., Srinivasan, M., Pochart, P., Qureshi-Emili, A., Li, Y., Godwin, B., Conover, D., Kalbfleisch, T., Vijayadamodar, G., Yang, M., Johnston, M., Fields, S., Rothberg, J.M.: A comprehensive analysis of protein–protein interactions in Saccharomyces cerevisiae. Nature 403, 623–627 (2000)
22. von Mering, C., Krause, R., Snel, B., Cornell, M., Oliver, S.G., Fields, S., Bork, P.: Comparative assessment of large-scale data sets of protein-protein interactions. Nature 417, 399–403 (2002)

Hirokazu Anai Katsuhisa Horimoto
Temur Kutsia (Eds.)

Algebraic Biology

Second International Conference, AB 2007
Castle of Hagenberg, Austria, July 2-4, 2007
Proceedings

Springer

Exact Parameter Determination for Parkinson's Disease Diagnosis with PET Using an Algebraic Approach

Hiroshi Yoshida[1], Koji Nakagawa[2], Hirokazu Anai[3], and Katsuhisa Horimoto[2]

[1] Faculty of Mathematics, Organization for the Promotion of Advanced Research, Kyushu University, Hakozaki 6-10-1, Higashi-ku, Fukuoka 812-8581 Japan
phiroshi@math.kyushu-u.ac.jp
[2] Computational Biology Research Centre (CBRC), National Institute of Advanced Industrial Science and Technology (AIST), Aomi 2-42, Koto-ku, Tokyo 135-0064, Japan
{nakagawa-koji,k.horimoto}@aist.go.jp
[3] IT Core Laboratories, FUJITSU LABORATORIES LTD./CREST, JST., Kamikodanaka 4-1-1, Nakahara-ku, Kawasaki 211-8588, Japan
anai@jp.fujitsu.com

Abstract. The mechanism of Parkinson's disease can be investigated at the molecular level by using radio-tracers. The concentration of dopamine in the brain can be observed by using a radio-tracer, 6-[^{18}F]fluorodopa (FDOPA), with positron emission tomography (PET), and the dopamine kinetics can be described as compartmental models for tissues of the brain. The models for FDOPA kinetics are solved explicitly, but the solution shows a complicated form including several convolutions over time domain. Owing to the complicated form of the solution, graphical analyses such as Logan or Patlak analysis have been utilized as conventional methods over past decades. Because some kinetic constants for Parkinson's disease are estimated in the graphical analyses with the slope or intercept of the line obtained under various assumptions, only a limited set of parameters have approximately been estimated. We have analysed the compartmental models by using the Laplace transformation of differential equations and by algebraic computation with the aid of Gröbner base constructions. We have obtained a rigorous solution with respect to the kinetic constants over the Laplace domain. Here, we first derive a rigorous solution for the parameters, together with a discussion about the merits of the derivation. Next, we describe a procedure to determine the kinetic constants with the observed time–radioactivity curves. Last, we discuss the feasibility of our method, especially as a criterion for diagnosing Parkinson's disease.

1 Introduction

Radio-tracers are often used to analyse metabolic systems in biomedical research. Usually the kinetics of metabolism are described as compartmental models, and kinetic constants are numerically estimated using the measurement of radio-tracers to diagnose the disease. In particular, the positron emission tomography (PET) has been developed to measure the details of metabolic events hitherto unavailable, and is especially useful to determine the kinetic constants to assist the diagnosis of various diseases.

H. Anai, K. Horimoto, and T. Kutsia (Eds.): AB 2007, LNCS 4545, pp. 110–124, 2007.

Parkinson's disease, which is due to abnormal levels of dopamine in the brain, is one of the diseases that can be diagnosed by radio-tracer measurement with PET, and by determination of kinetic constants in compartmental models for plasma and brain tissue [12]. There are two approaches to measuring the activity of radio-tracers. One is a combination of the measurement of a radio-tracer, L-3,4-dihydroxy-6-[^{18}F]fluoro-phenylalanine (FDOPA) in the brain, and sampling the blood to measure the total activity of FDOPA (approach with blood sampling), and the other is the measurement of the FDOPA activity in two brain tissues (approach without blood sampling). In both approaches, the kinetics can be described as sets of compartmental models. Fortunately, a system of differential equations in the two sets of models can be solved explicitly , but unfortunately the solutions for estimating the kinetic constants are highly complicated. Indeed, the solutions are expressed by a few convolutions of complicated equations.

To overcome analytical difficulties in determining kinetic constants, there are two conventional methods of kinetic constant estimation in the compartmental models, Patlak Analysis [18, 19] and Logan Analysis [15]. In both methods, the combination of some parameters with various approximations is assumed to form a straight line as metabolism approaches an equilibrium. By plotting the observed data around the metabolic equilibrium (graphical analysis), the combined parameters can be estimated using the slope or intercept in the plotted line [14, 18].

By using graphical analysis, Parkinson's disease has been extensively studied in the two approaches with and without the blood sampling. In the approach using blood sampling, the kinetic constants with respect to plasma are calculated from the blood-sampling data, and then, using these constants, measurements for Parkinson's disease such as the constants describing FDOPA kinetics in brain tissue are calculated [10, 11, 12, 20]. In addition, Martin et al. [16] considered L-3,4-dihydroxy-6-[^{18}F]fluoro-3-O-methylphenylalanine (3-OMFD) in compartmental models for FDOPA metabolism, because FDOPA is converted to 3-OMFD [1, 17], which has an influence on the total radioactivity observed in plasma and in the brain tissue by crossing the blood-brain barrier (BBB). In an approach without blood sampling, using the time–radioactivity curves of two distinct brain tissues, the constants for Parkinson's disease diagnosis are calculated [9, 14].

The diagnosis of Parkinson's disease with PET depends on graphical analysis, a simple presentation of the relationships between the kinetic constants of the FDOPA kinetics. However, the present analyses require further improvement for precise diagnoses. For example, graphical analysis using blood sampling is cumbersome, partly because the sampling requires a load to the patients, and partly because the separate measurement of radio-tracer from the blood provides an obstacle for the precise estimation of parameters such as the time delay and contamination of the samples in the tubing. Graphical analysis without blood sampling produces a highly complicated model and therefore requires various assumptions and approximations to estimate kinetic constants. Thus, the choice between the two approaches involves a trade-off between cumbersome blood sampling and difficult efficient parameter determination. Indeed, by considering the pitfalls described above, some methods have also designed by using different radio-tracers. For instance, Ichise et al. [8] proposed a method without blood sampling by using [^{123}I]iodobenzofuran, and Lammertsma et al. [13] and

Logan et al. [14] proposed a method without blood sampling by using [^{11}C]raclopride, in which the cerebellum or cerebral cortex was used as a reference tissue and analysed as a single-tissue compartment. Although the pitfalls have partially been overcome, a rigorous solution has not yet been analysed.

In this paper, we propose radical deliverance from the aforementioned difficulty. We present an efficient method for determining kinetic constants for FDOPA kinetics with PET using an algebraic approach. The compartmental models are rigorously solved by the Laplace transformation of differential equations into algebraic equations, and by the following symbolic computation with the aid of Gröbner bases. Such usage of symbolic computation has overcome the analytical difficulties in the previous study [6], where general theory of compartmental models was derived over the Laplace domain for PET, but the analysis or determination of kinetic constants still required the system's equilibrium or steady state. In our method, by contrast, the derivation of a relationship between the observed concentrations without blood sampling by PET does not need any approximations and assumptions for the kinetic constants. Here, we first derive rigorous relationships between the parameters, and we discuss the merits of the derivation, in comparison with graphical analyses. Second, we describe an efficient procedure for determining the kinetic constants with observed time–radioactivity curves. Last, we discuss the feasibility of our method, especially as a criterion for diagnosing Parkinson's disease.

2 Model and Method

In this section, we introduce three compartmental models to describe the metabolism of the radio-tracer FDOPA and its metabolites with respect to two brain tissues and plasma. Differential equations corresponding to the kinetic model are derived, and the equations are transformed into a system of algebraic equations. Surprisingly, the rigorous solution is of a simple form over the Laplace domain. Finally, we describe a procedure to determine the kinetic constants of the models, which is performed over the Laplace domain.

2.1 Compartmental Model

Compartmental models (A) and (B) are introduced for the radio-tracer FDOPA and its metabolite 3-OMFD as shown in Figs. 1 (a) and (b). For simplicity, let A- and B-tissues denote tissues in which the radio-tracer kinetics can be described as shown in Figs. 1 (a) and (b), respectively. In the actual brain, A- and B-tissues correspond to the striatum (putamen/caudate) and the cerebellum/cerebral cortex in the brain [4, 7]. Furthermore, it is assumed that the relationships between plasma FDOPA, 3-OMFD, and extra-vascular 3-OMFD can be described as the compartmental model (C) as shown in Fig. 1 (c).

2.2 Kinetic Equations

According to the kinetic model in Fig. 1, the following system of differential equations has been obtained:

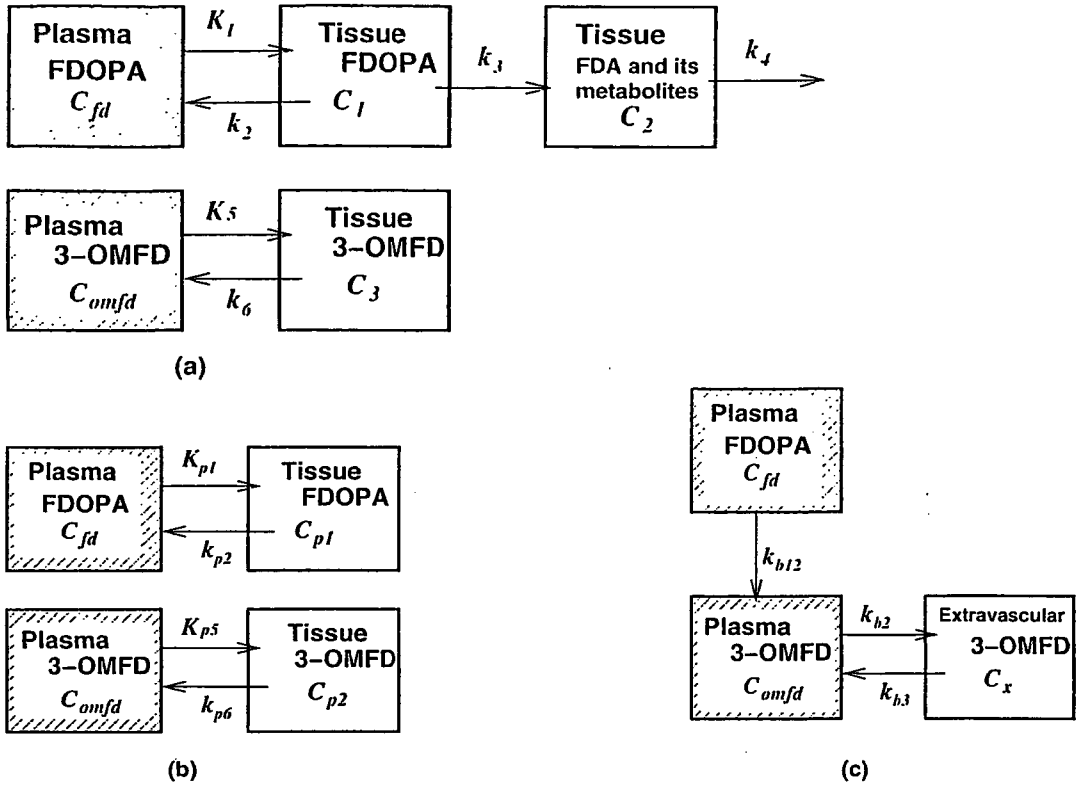

Fig. 1. Compartmental models for describing the radio-tracer kinetics in this paper, which were originally introduced by Huang et al. [7]. The shaded boxes represent the kinetics in plasma. (a) Model for A-tissue. Three separate compartments for tissue FDOPA, tissue FDA (and its metabolites), and tissue 3-OMFD. (b) Model for B-tissue which is the same as (a), except that there is no compartment for FDA. (c) Model for plasma FDOPA to 3-OMFD in the periphery of one compartment for plasma 3-OMFD and one for the extra-vascular pool.

Time (A-Tissue)

$$\begin{cases} \dfrac{dC_1}{dt} = K_1 C_{fd}(t-\tau)\theta(t-\tau) - (k_2+k_3)C_1, \\ \dfrac{dC_2}{dt} = k_3 C_1 - k_4 C_2, \\ \dfrac{dC_3}{dt} = K_5 C_{omfd}(t-\tau)\theta(t-\tau) - k_6 C_3, \end{cases} \tag{1}$$

Time (B-Tissue)

$$\begin{cases} \dfrac{dC_{p1}}{dt} = K_{p1} C_{fd}(t-\tau)\theta(t-\tau) - k_{p2} C_{p1}, \\ \dfrac{dC_{p2}}{dt} = K_{p5} C_{omfd}(t-\tau)\theta(t-\tau) - k_{p6} C_{p2}, \end{cases} \tag{2}$$

Time (C-Blood (Plasma))

$$\begin{cases} \dfrac{dC_{omfd}}{dt} = k_{b12}C_{fd} - k_{b2}C_{omfd} + k_{b3}C_x, \\ \dfrac{dC_x}{dt} = k_{b2}C_{omfd} - k_{b3}C_x. \end{cases} \tag{3}$$

In the compartmental model (A), (B), and (C), every one of the initial values is assumed to be zero because of non-existence of the radio-tracers and their metabolites at starting time $t = 0$. However, there exists the time delay τ of the observed blood curve (C) relative to tissue measurements (A) and (B). That is, τ designates a difference between the starting times of (A), (B), and (C). This effect leads to the terms $C_{fd}(t-\tau)\theta(t-\tau)$ and $C_{omfd}(t-\tau)\theta(t-\tau)$, where $\theta(t)$ is the unit step function defined as follows:

$$\theta(t) = \begin{cases} 0 & (t < 0), \\ 1 & (t > 0). \end{cases}$$

The differential equations describing the A- and B-tissues and the C-blood kinetics models can be changed into the following equations over the Laplace domain:

Laplace (A)

$$\begin{cases} sL[C_1] = K_1 e^{-s\tau}L[C_{fd}] - (k_2 + k_3)L[C_1], \\ sL[C_2] = k_3 L[C_1] - k_4 L[C_2], \\ sL[C_3] = K_5 e^{-s\tau}L[C_{omfd}] - k_6 L[C_3], \end{cases} \tag{4}$$

Laplace (B)

$$\begin{cases} sL[C_{p1}] = K_{p1} e^{-s\tau}L[C_{fd}] - k_{p2}L[C_{p1}], \\ sL[C_{p2}] = K_{p5} e^{-s\tau}L[C_{omfd}] - k_{p6}L[C_{p2}], \end{cases} \tag{5}$$

Laplace (C)

$$\begin{cases} sL[C_{omfd}] = k_{b12}L[C_{fd}] - k_{b2}L[C_{omfd}] + k_{b3}L[C_x], \\ sL[C_x] = k_{b2}L[C_{omfd}] - k_{b3}L[C_x], \end{cases} \tag{6}$$

where $L[f]$ denotes the Laplace transformation of f. Thus, a system of differential equations is transformed into a system of corresponding algebraic equations.

2.3 Rigorous Solution

In the approach without blood sampling, the data observed using PET scanning are limited to the total radioactivities: $Cs(t) = C_1(t) + C_2(t) + C_3(t)$ and $Cc(t) = C_{p1}(t) + C_{p2}(t)$. Let $Cs(s)$ and $Cc(s)$ denote the Laplace transformations of $Cs(t)$ and $Cc(t)$, respectively. Then, the solution to the system of algebraic equations of Laplace (A),

(B), and (C) has been obtained, leading to a rigorous and simple relationship between $Cs(s)$ and $Cc(s)$ as follows:

$$\frac{Cs(s)}{Cc(s)} = \frac{(s+k_{p2})(s+k_{p6})}{(s+k_2+k_3)(s+k_4)(s+k_6)} \times \frac{K_5 k_{b12}(s+k_2+k_3)(s+k_4)(s+k_{b3}) + sK_1(s+k_3+k_4)(s+k_6)(s+k_{b2}+k_{b3})}{K_{p5}k_{b12}(s+k_{b3})(s+k_{p2}) + sK_{p1}(s+k_{b2}+k_{b3})(s+k_{p6})}. \quad (7)$$

Thus, $Cs(s)/Cc(s)$ is a rational function in s to which symbolic methods such as Gröbner base computations can be applied, resulting in exact and efficient parameter determination.

2.4 Procedure to Determine the Kinetic Constants

Procedure overview. Fig. 2 shows an overview of the present procedure for determining the kinetic constants from radio-tracer activity data. The procedure is composed of two parts. First, we fit the observed radioactivity curves by a series of exponentials, and then the fitted series of exponentials are transformed into the corresponding algebraic equations by the Laplace transformation. Second, the kinetic constants in the rigorous equation (7) are determined using an algebraic approach. The details of the above procedure are described below.

Laplace transformation of the observed data. We need a Laplace transformation of the observed data because we perform parameter determination over the Laplace domain. Let $Cso(t)$ and $Cco(t)$ denote the observed data in A- and B-tissues, respectively. By using non-linear regression, $Cso(t)$ and $Cco(t)$ are expressed in terms of a series of exponentials according to [3] as follows:

$$\begin{cases} Cso(t) = a_1 \exp(-m_1 t) + a_2 \exp(-m_2 t) - (a_1 + a_2 + aa)\exp(-m_3 t) + aa, \\ Cco(t) = b_1 \exp(-l_1 t) + b_2 \exp(-l_2 t) - (b_1 + b_2 + bb)\exp(-l_3 t) + bb, \end{cases} \quad (8)$$

where the initial values are assumed to be zero, namely $Cso(0) = 0$ and $Cco(0) = 0$ because of non-existence of radio-tracer at $t = 0$ as mentioned in §2.2. However, this assumption has an inference on regression of the parameters: a_i, b_i, aa, bb, m_i and l_i owing to inaccuracy or noise in the observed data that leads to $Cso(0) \neq 0$ or $Cco(0) \neq 0$. To avoid this inference, we have adopted an additional value: η. We have firstly fitted the observed data with $Cso(t-\eta)$ and $Cco(t-\eta)$, and then have substituted η with 0, that is, η has been ignored. $Cso(t)$ and $Cco(t)$ thus fitted are changed into the Laplace-transformed data as follows:

$$\begin{cases} L[Cso(t)] = \dfrac{a_1}{s+m_1} + \dfrac{a_2}{s+m_2} - \dfrac{a_1+a_2+aa}{s+m_3} + \dfrac{aa}{s}, \\ L[Cco(t)] = \dfrac{b_1}{s+l_1} + \dfrac{b_2}{s+l_2} - \dfrac{b_1+b_2+bb}{s+l_3} + \dfrac{bb}{s}, \end{cases} \quad (9)$$

where L denotes the Laplace transformation.

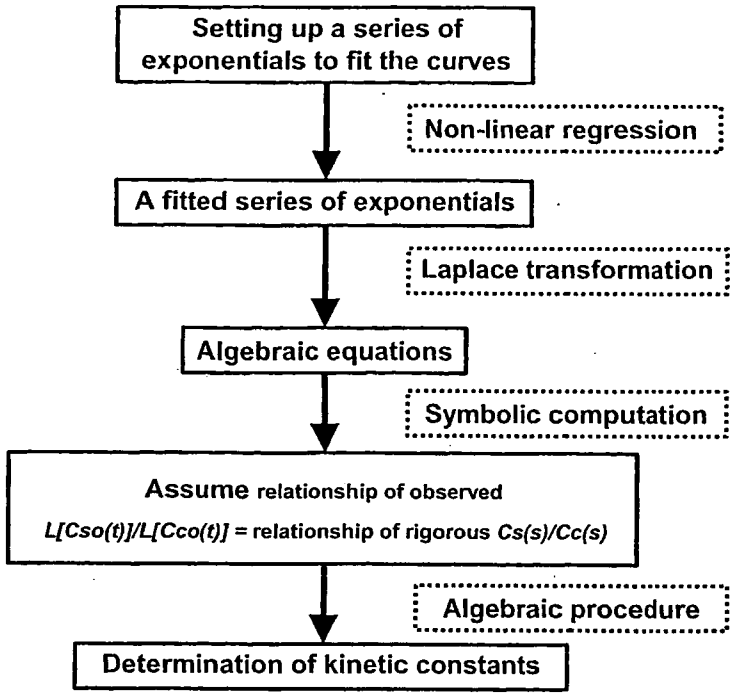

Fig. 2. Overview of the procedure for determining kinetic constants

Algebraic procedure. Without any error, the transformed function of A-tissue data, $L[Cso(t)](s)$, and that of B-tissue data, $L[Cco(t)]$, would be identical with $Cs(s)$ and $Cc(s)$, respectively. This fact has led us to the following procedure to determine the parameters over the Laplace domain.

1. $L[Cso(t)]/L[Cco(t)]$ can be transformed into the form: $F(s)/G(s)$, where $F(s)$ and $G(s)$ are both fifth-order polynomials in s. It follows from Eq. (7) that $-(k_2 + k_3)$, $-k_4$, and $-k_6$ are three of the real roots of $G(s)$. Likewise, $-k_{p2}$ and $-k_{p6}$ are two of the real roots of $F(s)$. It can be proved that both $F(s)$ and $G(s)$ have five real negative roots in PET experiments as mentioned in Appendix A.
2. Let $-r_i$ $(1 \leq i \leq 5)$ and $-t_i$ $(1 \leq i \leq 5)$ denote the real roots of $F(s)$ and $G(s)$, respectively. From (1), $k_2 + k_3$, k_4, and k_6 are three of t_i, e.g., t_1, t_2, and t_3. Likewise, k_{p2} and k_{p6} are, e.g., r_1 and r_2. The number of assignments of the parameters $k_2 + k_3, k_4, k_6, k_{p2}$, and k_{p6} to r_i and t_i is 1200. We apply these 1200 assignments to the two procedures below.
3. The remaining parameters, $K_1/K_{p1}, K_5k_{b12}/K_{p1}, K_{p5}k_{b12}/K_{p1}, k_2, k_3, k_{b2}$, and k_{b3}, are calculated by solving the following system of algebraic equations:

$$H(-r_3) = H(-r_4) = H(-r_5) = I(-t_4) = I(-t_5) = 0,\ k_2 + k_3 = t_1,$$
$$K_1/K_{p1} = HC(F(s))/HC(G(s)),$$

where $H(s) = K_5k_{b12}(s+k_2+k_3)(s+k_4)(s+k_{b3})+sK_1(s+k_3+k_4)(s+k_6)(s+k_{b2}+k_{b3})$, $I(s) = K_{p5}k_{b12}(s + k_{b3})(s + k_{p2}) + sK_{p1}(s + k_{b2} + k_{b3})(s + k_{p6})$, and HC denotes the

head coefficient. To solve the system of algebraic equations above, we have derived the triangular form with the aid of Gröbner base computations. The third-order polynomial as the elimination ideal with respect to k_{b3} is shown in Appendix B.

4. Because the numerator and denominator of $Cs(s)/Cc(s)$ (Eq. (7)) are both sixth-order polynomials in s while $F(s)$ and $G(s)$ are both fifth-order, the similarity between $Cs(s)/Cc(s)$ and $F(s)/G(s)$ can be calculated by the difference between the roots of the numerator and denominator of $Cs(s)/Cc(s)$ that do not appear as the roots of $F(s)$ or $G(s)$. These two roots are calculated by coefficient comparison as follows:

$$k_3+k_4+k_6+k_{b2}+k_{b3}+K_5k_{b12}/K_1-(r_3+r_4+r_5),\ k_{b2}+k_{b3}+k_{p6}+K_{p5}k_{b12}/K_{p1}-(t_4+t_5).$$

We record the difference between the above two roots as *diff*. Notice that the roots of $F(s)$ and $G(s)$ correspond to the reciprocals of time constants of PET experiments and that they are distinct from one another.

5. The parameter sets determined above are arranged in ascending order by *diff*. Furthermore, we remove parameter sets that violate an empirical or physiological law. In this paper, we have adopted the following law:

$$k_{p2} < k_{p6} \text{ and } k_3 < 1. \tag{10}$$

The first inequality, $k_{p2} < k_{p6}$, designates a different permeability of FDOPA and 3-OMFD, which cross the BBB (blood-brain barrier) [5, 7]. The second inequality, $k_3 < 1$, is the empirical law.

6. The result of the procedure above is the first parameter set among the sets in ascending order by *diff*.

Using the procedure described above, we can immediately and effectively determine the parameters such that all of them are consistent with PET experiments.

3 Results

We have extracted the observed data of A- and B-tissues from Cumming and Gjedde [4, p.52, Fig. 4], where A- and B-tissues correspond to the caudate and the cerebral (occipital) cortex, respectively. First, we have fitted the ^{18}F radioactivity data in A- and B- tissues of the normal control subject and the patient with Parkinson's disease (PD) as a series of exponentials according to $Cso(t-\eta_A)$ and $Cco(t-\eta_B)$ in Eq. (8). The parameters obtained, $a_i, b_i, aa, bb, m_i, l_i$, are represented in Table 1. Figure 3 shows the fitting of the observed data. As seen in Fig. 3, the estimated curves are fitted from control and PD patient samples.

By using the parameters in Table 1, we have obtained kinetic constants according to the algebraic procedure in §2.4. This calculation needed 15 seconds CPU time and 5.5 MBytes memory via Mathematica 5.2 (Wolfram Research, Inc.) with Intel(R) Xeon(R) CPU 2.33GHz. Table 2 shows almost all kinetic constants of the control and PD patient,

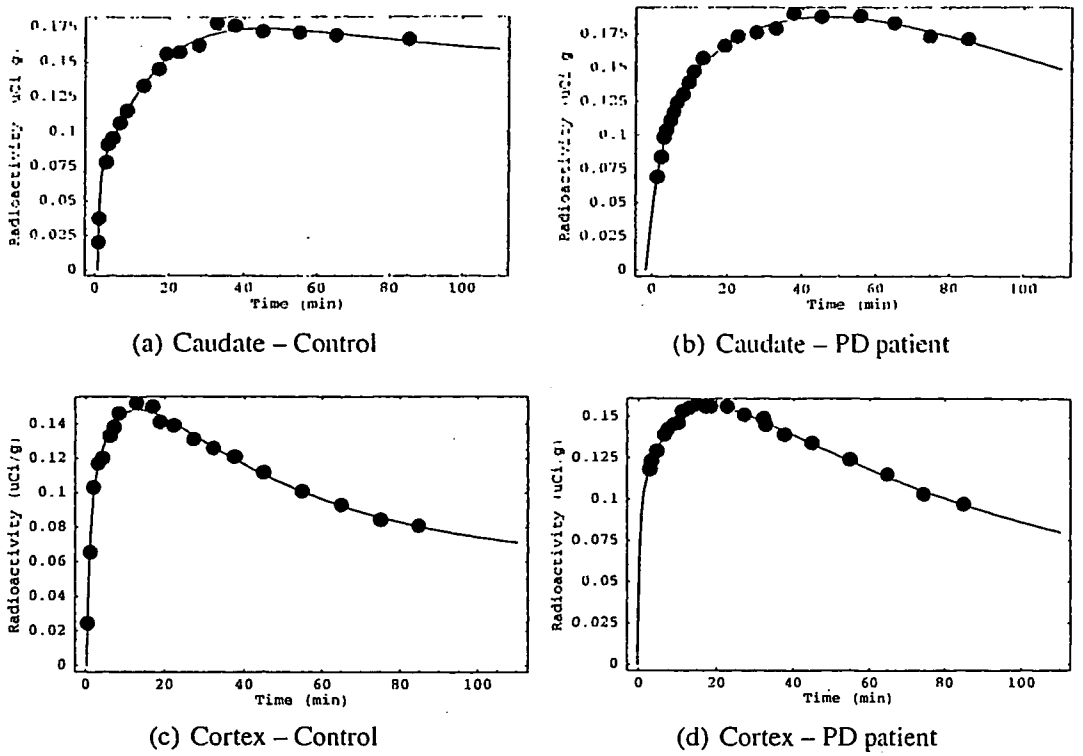

(a) Caudate – Control

(b) Caudate – PD patient

(c) Cortex – Control

(d) Cortex – PD patient

Fig. 3. Time–radioactivity curves in the occipital cortex and caudate of a patient with Parkinson's disease and a normal control subject during 90 min after administration of [^{18}F]fluorodopa. The circles are the observed data that have been extracted from [4, p.52, Fig. 4], and the solid curves are fits by a series of exponentials. (a) Radioactivity in caudate of a normal control subject. (b) Caudate of a patient with Parkinson's disease. (c) Occipital cortex of the control. (d) Occipital cortex of the patient.

in comparison with those in the previous estimation [4]. First, we have determined almost all values of kinetic constants, while the previous work only partially estimated the constants, using graphical analysis. Second, the orders of the kinetic constants obtained by our method are similar to those found by the graphical analysis, for both the control and PD patient. Interestingly, one constant, k_4, which is one of the measures for Parkinson's disease, was slightly different but consistent in our analysis compared with that in the previous study. The difference/consistency of the constants in the two studies will be judged from future work where many samples are analysed. At any rate, we have successfully determined almost all constants without blood-sampling data via our method.

4 Discussion

We have derived the equation Eq. (7), which enables us to determine rigorously almost all of the kinetic constants in the FDOPA model. In contrast, graphical analysis can only approximately determine the kinetic constants around the equilibrium of the

Table 1. The obtained parameters by non-linear regression

A-tissue ($Cso(t-\eta_A)$)	a_1	a_2	aa	m_1	m_2	m_3	η_A
Control	−0.0660074	−4.66107	0.153617	2.31191	0.0399169	0.038911	0.893464
PD patient	−0.10455	−3.02326	0.0588441	0.275661	0.0183807	0.0166495	−1.49546
B-tissue ($Cco(t-\eta_B)$)	b_1	b_2	bb	l_1	l_2	l_3	η_B
Control	−0.0826722	−0.11201	0.058033	1.31972	0.16269	0.021298	0.298255
PD patient	−0.0928105	−0.107709	0.0252521	2.05784	0.113904	0.0105398	−0.267787

Table 2. Kinetic constants of control and PD patient in FDOPA model by the procedure in §2.4 *without* blood–sampling data. The figures in the square bracket denote k_4 by Patlak analysis *with* blood–sampling data [4].

Kinetic constants	k_2	k_3	k_4	k_6	k_{p2}	k_{p6}	k_{b2}	k_{b3}
Control	0.0968	0.220	0.00674 [0.011 ± 0.003]	0.0389	0.0213	1.32	0.0525	0.00122
PD Patient	0.000818	0.0176	0.0166 [0.016 ± 0.004]	0.276	0.00231	0.0646	0.0276	0.112

(Continue)	K_1/K_{p1}	K_5k_{b12}/K_{p1}	$K_{p5}k_{b12}/K_{p1}$
Control	1.29	0.0466	0.979
PD Patient	0.165	0.291	0.120

system under various assumptions and ignorance [6]. For instance, even the striatum (corresponding to A-tissue in this paper) was modelled as a single-tissue compartment [9]. Moreover, replacement with averaged values and ignorance of error terms as a small value are required for the solution to the equation over time domain because of its complicated form. Thus, the present method by the algebraic approach has successfully overcome the difficulties of graphical analysis.

Apart from graphical analyses, Cobelli et al. [2, 3] have studied the relationship between the observational parameters and the unknown model parameters over the Laplace domain. The aim of these works was determination of a model in which, on the assumption that any noise does not exist, it is determined whether the parameters can be determined uniquely or non-uniquely. In contrast, in this paper, we have determined parameters from the observed data with noise via the algebraic procedure as mentioned in §2.4. One of the other procedures to determine parameters from noisy data is the least squares method. We have attempted the least squares method using the following equation:

$$\int_{ls}^{us} (Cs(s)L[Cco(t)](s) - Cc(s)L[Cso(t)](s))^2 \mathbf{d}s.$$

Although the selection of interval between ls and us is somewhat ambiguous and it takes about 2.7 hours for each simulation with AMD Opteron(tm) Processor 2.412GHz, this method usually brings us the same results as the algebraic procedure and might be suitable for the equation where blood vessels in tissues are taken into account.

The solution over the Laplace domain is an algebraic equation to which Gröbner base computations can be applied, resulting in a much simpler form and efficient parameter

determination (about 15 seconds with Intel(R) Xeon(R) CPU 2.33GHz). In fact, the equivalent equation to Eq. (7) can be described over time domain as follows:

$$\begin{aligned} C_s(t) &= C_c(t) \otimes Y_1(t) \otimes Y_2(t), \\ \text{with } Y_1(t) &= \frac{(k_2+k_3-k_{p2})(k_2+k_3-k_{p6})}{(k_2+k_3-k_4)(k_2+k_3-k_6)} e^{-(k_2+k_3)t} \\ &\quad - \frac{(k_4-k_{p2})(k_4-k_{p6})}{(k_2+k_3-k_4)(k_4-k_6)} e^{-k_4 t} - \frac{(k_6-k_{p2})(k_6-k_{p6})}{(k_2+k_3-k_6)(k_6-k_4)} e^{-k_6 t}, \\ Y_2(t) &= \text{Extremely complicated formula over time domain} \\ &\quad \text{(shown in Supplementary material)}, \end{aligned} \tag{11}$$

where $\otimes$ denotes the mathematical operation of convolution. The point is that we have solved the system of differential equations over the Laplace domain. In general, the solution including any external force over time domain (in this paper, C_{fd} in the C-Blood model is the external force) leads to the mathematical operation of 'convolution.' Instead, convolution over time domain corresponds to a simpler form of multiplication over the Laplace domain.

Lastly, we note that the present approach can be applied to more complex compartmental models. In compartmental models, the Laplace transformation of differential equations into algebraic equations and the following symbolic computation will reveal a rigorous relationship between kinetic constants. Furthermore, the algebraic procedure seems useful for determining constants from data.

5 Conclusion

We have derived a rigorous relationship for the kinetic constants of compartmental models for FDOPA metabolism, by symbolic computations with the aid of Gröbner bases. The algebraic procedure has successfully determined almost all constants from the observed radioactivity curves. In particular, the rigorous and simple form of a solution for the constants relationship brings us efficient parameter determination *without* blood-sampling data and *only from* PET scanning data that are dozens of minutes short of the equilibrium leading to the considerable reduction of PET scanning periods required for diagnosis.

Acknowledgment

We wish to express our gratitude to Ms. Atsuko Sono and Mr. Shigeo Orii for their supports. H. Y. and K. H. were partly supported by a Grant-in-Aid for Scientific Research on Priority Areas "Systems Genomics" (grant 18016008) from the Ministry of Education, Culture, Sports, Science and Technology of Japan. This study was supported in part by the New Energy and Industrial Technology Development Organization (NEDO) of Japan, and by The Kyushu University Research Superstar Program (SSP) from Special Coordination Funds for Promoting Science and Technology of Japan Science and Technology Agency (JST).

References

[1] Boyes, B.E., Cumming, P., Martin, W.R.W., Macgeer, E.G.: Determination of plasma [^{18}F]-6-fluorodopa during positron emission tomography: elimination and metabolism in carbidopa treated subjects. Life Sci. 39, 2243–2252 (1986)

[2] Cobelli, C., Foster, D., Toffolo, G.: Tracer Kinetics in Biomedical research: From data to model. Kluwer Academic/Plenum Publishers (2000)

[3] Cobelli, C., Toffolo, G.: Theoretical aspects and practical strategies for the identification of unidentifiable compartmental systems. In: chapter 8, pp. 85–91. Pergamon Press, Oxford (1987)

[4] Cumming, P., Gjedde, A.: Compartmental Analysis of Dopa Decarboxylation in living brain from dynamic positron emission tomograms. Synapse 29, 37–61 (1998)

[5] Deep, P., Kuwabara, H., Gjedde, A., Cumming, P.: The kinetic behaviour of [^{3}H]DOPA in living rat brain investigated by compartmental modelling of static autoradiograms. J. Neurosci. Methods 78, 157–168 (1997)

[6] Gunn, R.N., Gunn, S.R., Cunningham, V.J.: Positron emission tomography compartmental models. J. Cereb. Blood Flow Metab. 21, 635–652 (2001)

[7] Huang, S.C., Yu, D.C., Barrio, J.R., Grafton, S., Melega, W.P., Hoffman, J.M., Satyamurthy, N., Mazziotta, J.C., Phelps, M.E.: Kinetics and Modeling of L-6-[^{18}F]Fluoro-DOPA in Human Positron Emission Tomographic Studies. J. Cereb. Blood Flow Metab. 11, 898–913 (1991)

[8] Ichise, M., Ballinger, J.R., Golan, H., Vines, D., Luong, A., Tsai, S., Kung, H.F.: SPECT imaging of dopamine D2 receptors in humans with iodine 123–IBF: a practical approach to quantification not requiring blood sampling. J. Nucl. Med. 36, 11 (1995)

[9] Kawatsu, S., Kato, T., N.-Saito, A., Hatano, K., Ito, K., Ishigaki, T.: New insight into the analysis of 6-[^{18}F]fluoro-L-DOPA PET dynamic data in brain tissue without an irreversible compartment: comparative study of the Patlak and Logan Analyses. Radiation medicine 21, 47–54 (2003)

[10] Kumakura, Y., Danielsen, E.H., Reilhac, A., Gjedde, A., Cumming, P.: Levodopa effect on [^{18}F]fluorodopa influx to brain: normal volunteers and patients with Parkinson's disease. Acta Neurol. Scand. 110, 188–195 (2004), doi:10.1111/j.1600-0404.2004.00299.x

[11] Kumakura, Y., Gjedde, A., Danielsen, E.H., Christensen, S., Cumming, P.: Dopamine storage capacity in caudate and putamen of patients with early Parkinson's disease: correlation with asymmetry of motor symptoms. J. Cereb. Blood Flow Metab. 26, 358–370 (2006), doi:10.1038/sj.jcbfm.9600202

[12] Kumakura, Y., Vernaleken, I., Gründer, G., Bartenstein, P., Gjedde, A., Cumming, P.: PET studies of net blood–brain clearance of FDOPA to human brain; age–dependent decline of [^{18}F]fluorodopamine storage capacity. J. Cereb. Blood Flow Metab. 25, 807–819 (2005), doi:10.1038/sj.jcbfm.9600079

[13] Lammertsma, A.A., Bench, C.J., Hume, S.P., Osman, S., Gunn, K., Brooks, D.J., Frackowiak, R.S.J.: Comparision of methods for analysis of clinical [^{11}C]Raclopride studies. J. Cereb. Blood Flow Metab. 16, 42–52 (1996)

[14] Logan, J., Fowler, J.S., Volkow, N.D., Wang, G.-J., Ding, Y.-S., Alexoff, D.L.: Distribution Volume Ratios without blood sampling from graphical analysis of PET Data. J. Cereb. Blood Flow Metab. 16, 834–840 (1996), doi:10.1097/00004647-199609000-00008

[15] Logan, J., Fowler, J.S., Volkow, N.D., Wolf, A.P., Dewey, S.L., Schlyer, D.J., MacGregor, R.R., Hitzemann, R., Bendriem, B., Gatley, S.J., Christman, D.R.: Graphical analysis of reversible radioligand binding from time–activity measurements applied to [N-^{11}C-methyl]-(–)-Cocaine PET studies in human subjects. J. Cereb. Blood Flow Metab. 10, 740–747 (1990)